Open Access Library Journal
2026, Volume 13, e14922
ISSN Online: 2333-9721
ISSN Print: 2333-9705

Graph Neural Networks for Modelling Emotion Regulation Pathways from Multimodal Wearable Signals

Rocco de Filippis[1]*, Abdullah Al Foysal[2]

[1]Department of Neuroscience, Institute of Psychopathology, Rome, Italy
[2]Department of Computer Engineering (AI), University of Genova, Genova, Italy
Email: *roccodefilippis@istitutodipsicopatologia.it, niloyhasanfoysal440@gmail.com

How to cite this paper: de Filippis, R. and Al Foysal, A. (2026) Graph Neural Networks for Modelling Emotion Regulation Pathways from Multimodal Wearable Signals. *Open Access Library Journal*, **13**: e14922.
https://doi.org/10.4236/oalib.1114922

Received: January 23, 2026
Accepted: March 15, 2026
Published: March 18, 2026

Abstract

Emotion regulation emerges from coordinated dynamics across autonomic, cardiovascular, electrodermal, thermoregulatory, and motor systems. Although wearable devices can continuously capture these signals, most predictive models either analyse each modality in isolation or fuse them via simple feature concatenation, which obscures the structured cross-system interactions that likely underpin successful regulation. We introduce a graph neural network (GNN) framework that encodes multimodal wearable physiology as a subject-specific graph: nodes represent physiological subsystems (ECG, EDA, PPG, accelerometery, skin temperature, and HRV), and edges model functional coupling estimated from modality-level feature similarity. To enable controlled benchmarking, we generate a synthetic but physiologically plausible dataset of 150 subjects spanning three affective states (negative, positive, regulated) and derive regulation-success labels using a physiology-informed rule based on HRV and sympathovagal balance (LF/HF). A hybrid GCN-GAT architecture achieves strong held-out performance (accuracy = 0.967, AUC = 0.982, F1 = 0.982) and exceeds reference baselines in a comparative evaluation. Beyond prediction, we include attention-based interaction analysis, although the current configuration does not reveal distinct regulation circuits analyses via attention-based node and edge scoring, facilitating inspection of candidate regulation circuits across systems. Finally, we outline key barriers to translation including synthetic-only validation, class-imbalance sensitivity, and potential attention degeneracy and propose methodological steps required for robust deployment on real-world wearable emotion regulation cohorts.

Subject Areas

Explainable Clinical AI

Keywords

Wearable Sensing, Emotion Regulation, Graph Neural Networks, Multimodal Physiology, ECG, EDA, HRV, Explainable AI, Digital Phenotyping

1. Introduction

Emotion regulation (ER), the capacity to monitor, evaluate, and modify emotional responses in order to achieve adaptive goals, is a fundamental mechanism supporting psychological well-being [1]-[6]. Disruptions in ER are implicated in a wide range of psychiatric and neurological conditions, including major depressive disorder, anxiety disorders, post-traumatic stress disorder, and bipolar spectrum disorders [7]-[16]. From a physiological perspective, ER does not arise from a single biological process; rather, it reflects the coordinated activity of multiple interacting subsystems encompassing autonomic, cardiovascular, electrodermal, thermoregulatory, and motor control processes [17]-[22].

Recent advances in wearable sensing technology now allow these subsystems to be observed continuously and non-invasively. Signals such as electrocardiography (ECG), electrodermal activity (EDA), photoplethysmography (PPG), body accelerometer (ACC), and peripheral skin temperature (TEMP) provide complementary information about autonomic balance, cardiovascular function, sympathetic arousal, behavioural activation, and metabolic regulation [23]-[33]. Together, these signals offer an unprecedented opportunity to characterize emotion regulation as a distributed physiological process unfolding in real time. However, despite the multimodal richness of wearable data, most existing computational models treat each modality either independently or as part of a flat concatenated feature vector. Such representations fail to explicitly encode the structured interdependencies among physiological systems that are central to effective emotion regulation.

In contrast, emotion regulation is inherently network-based: successful regulation is marked by patterns such as parasympathetic rebound in cardiac dynamics, concurrent suppression of electrodermal arousal, stabilization of motor activity, and gradual normalization of thermal responses [34]-[39]. Capturing these interactions requires a modelling paradigm capable of representing both individual physiological dynamics and their relational organization. Graph learning provides a natural and principled solution to this problem. By modelling physiological subsystems as nodes and their functional relationships as edges, graph neural networks (GNNs) can learn representations that explicitly encode cross-system coordination while remaining amenable to mechanistic interpretation through attention mechanisms and edge-level analysis [40]-[46].

In this work, we propose a novel GNN-based framework for modelling emotion regulation from multimodal wearable signals [47]-[50]. We represent each subject's physiological state as a subject-specific graph comprising six interacting subsystems (ECG, EDA, PPG, ACC, TEMP, HRV), with edge weights derived from functional coupling between modality-specific feature representations [51]-[56]. To support controlled experimentation and reproducibility, we introduce a physiologically grounded synthetic data generator that produces realistic wearable time series under distinct affective states. We then train a hybrid GCN-GAT architecture to predict emotion regulation success and provide interpretable pathway analyses that reveal candidate regulation circuits across physiological systems [57]-[60].

Contributions

This paper makes the following key contributions:

1. Multimodal Wearable Data Generator: We develop a physiologically informed synthetic data engine that produces realistic ECG, EDA, PPG, ACC, and TEMP time series with affect-specific parameterization and noise characteristics.

2. Physiology-Driven Graph Representation: We introduce a subject-level physiological graph with six interacting subsystems and edge weights encoding functional coupling between modalities.

3. Hybrid GNN Architecture: We propose a GNN model combining stacked graph convolutional layers with graph attention for robust prediction of emotion regulation success.

4. Comprehensive Experimental Evaluation: We conduct extensive validation using train/validation/test splits, confusion matrices, ROC-AUC analysis, and attention-based interpretability.

5. Interpretable Pathway Analysis Tools: We provide visualization and analysis techniques that expose cross-system interaction pathways underlying emotion regulation.

This framework establishes a principled foundation for modelling emotion regulation as a networked physiological process and lays the groundwork for future clinically deployable wearable emotion regulation systems.

2. Related Work

Computational modelling of affect and emotion regulation using wearable devices has evolved substantially over the past decade, driven by rapid advances in sensor technology and machine learning [61]-[66]. Early studies primarily focused on heart rate variability (HRV) and electrodermal activity (EDA) as robust indicators of autonomic arousal, stress, and emotional intensity, with extensive evidence linking vagal tone and sympathetic activation to affective state transitions. Subsequent work expanded this univariate paradigm to include additional modalities such as photoplethysmography (PPG), body accelerometery, and peripheral skin temperature, enabling richer characterization of emotional and behavioural responses in naturalistic environments [67]-[71].

From a modelling perspective, two dominant approaches have emerged. Classical pipelines rely on hand-crafted physiological descriptors such as time- and frequency-domain HRV metrics, EDA tonic and phasic components, pulse morphology indices from PPG, and movement statistics followed by conventional classifiers including logistic regression, support vector machines, and random forests. In parallel, deep learning methods have increasingly been applied directly to raw or minimally processed time series using convolutional neural networks (CNNs), recurrent architectures (LSTMs, GRUs), and more recently Transformer-based models [72]-[78]. These approaches demonstrate strong performance in emotion and stress recognition tasks but typically treat multimodal fusion as either feature concatenation or late-stage ensemble learning, thereby limiting their ability to explicitly model structured cross-system interactions.

More recently, graph-based learning has emerged as a promising paradigm for multimodal bio-signal analysis. By representing each physiological modality as a node and defining edges according to functional or statistical relationships, graph neural networks provide a principled framework for encoding physiological priors, integrating heterogeneous feature spaces, and learning interaction patterns that are both predictive and interpretable. Graph formulations have been applied to EEG-based affect decoding, multimodal health monitoring, and cross-sensor fusion problems, demonstrating improved generalization and robustness compared to flat feature models. Importantly, GNNs support explainability through node- and edge-level importance measures, enabling the extraction of candidate physiological pathways underlying observed behavioural states.

Despite these advances, the application of graph learning to emotion regulation remains largely unexplored. Most existing studies focus on emotion classification or stress detection rather than the regulation process itself, and few explicitly model the coordinated physiological dynamics that characterize successful emotional control. Our work extends this emerging literature by framing emotion regulation as an emergent network-level phenomenon, in which regulatory success is encoded in the structured interactions among cardiovascular, autonomic, electrodermal, thermal, and motor subsystems. By combining multimodal wearable sensing with graph neural modelling and pathway-level interpretability, we introduce a novel computational perspective on emotion regulation that bridges physiological theory with modern representation learning.

3. Methods

3.1. Synthetic Wearable Dataset

To enable controlled evaluation and reproducible experimentation, we constructed a physiologically grounded synthetic dataset comprising 150 virtual subjects, equally distributed across three affective conditions: negative, positive, and regulated (50 subjects per state). For each subject, we generated synchronized multimodal wearable signals sampled at 64 Hz over 2000 timepoints, corresponding to approximately 31 seconds of continuous recording per subject. The dataset

includes five primary modalities: electrocardiography (ECG), electrodermal activity (EDA), photoplethysmography (PPG), tri-axial accelerometery (ACC), and peripheral skin temperature (TEMP).

This synthetic framework allows systematic manipulation of affective and physiological parameters while preserving realistic signal morphology and cross-modal coherence, thereby providing a stable testbed for modelling emotion regulation dynamics [79]-[85].

3.1.1. Physiologically Informed Signal Generation

Each affective state was parameterized using empirically motivated physiological profiles reflecting established psychophysiological findings:

- Negative affect was modelled by elevated mean heart rate, increased heart-rate variability amplitude, heightened electrodermal baseline with frequent skin conductance responses (SCR-like transients), agitated and irregular motor activity, and mildly increased thermal variability.
- Positive affect exhibited moderate heart rate and electrodermal activity, rhythmic and coordinated movement patterns, and stable peripheral temperature dynamics.
- Regulated affect was characterized by reduced heart-rate variability amplitude, low electrodermal baseline with minimal phasic responses, calm and steady motor behaviour, and highly stable thermal regulation.

Signal synthesis followed modality-specific generative processes:

Electrocardiography (ECG): ECG signals were constructed using a simplified physiological cardiac model composed of Gaussian-shaped P, QRS, and T wave components. Instantaneous heart rate varied over time according to affect-specific parameters and low-frequency oscillations, with additive Gaussian noise applied to simulate sensor artifacts and biological variability.

Electrodermal Activity (EDA): EDA was generated as the superposition of a tonic baseline, slow oscillatory drift, and discrete phasic events representing SCRs. The frequency, amplitude, and temporal dispersion of SCR-like transients were modulated according to affective state, with negative affect producing the highest density of phasic responses.

Photoplethysmography (PPG): PPG waveforms were synthesized as harmonically modulated sinusoids synchronized with instantaneous heart rate, incorporating higher-order harmonics and stochastic noise to approximate realistic pulse morphology.

Accelerometer (ACC): Tri-axial accelerometer signals were modelled as low-frequency sinusoidal motion components combined with state-dependent Gaussian noise. Negative affect produced irregular, high-variance movement; positive affect yielded rhythmic, moderate activity; and regulated affect generated low-amplitude, highly stable motion profiles.

Skin Temperature (TEMP): Temperature dynamics were simulated as a slow-varying baseline with low-frequency oscillations and affect-dependent modulation. Negative affect introduced increased variability consistent with stress-related

vasomotor effects, while regulated affect produced near-stationary thermal behaviour.

Together, these generative mechanisms produce multimodal wearable data exhibiting realistic morphology, variability, and cross-modal coupling while allowing precise experimental control over affective and regulatory conditions.

3.1.2. Heart Rate Variability (HRV) Feature Extraction

To quantify autonomic regulation dynamics, heart rate variability (HRV) features were extracted from the synthesized ECG signals. R-peak locations were first approximated using a peak detection algorithm applied to the ECG waveform. The resulting sequence of R-R intervals was converted to milliseconds and used to compute standard time-domain HRV metrics.

Specifically, we calculated:

- **Root Mean Square of Successive Differences (RMSSD)**

$$\mathrm{RMSSD} = \sqrt{\mathbb{E}\left[\left(\Delta RR\right)^2\right]}$$

which reflects short-term parasympathetic activity and is strongly associated with emotional regulation capacity.

- **Standard Deviation of Normal-to-Normal intervals (SDNN)**

$$\mathrm{SDNN} = \mathrm{Std}\left(RR\right)$$

which captures overall heart rate variability.

To approximate frequency-domain autonomic balance, low-frequency (LF) and high-frequency (HF) components were generated as physiologically plausible stochastic proxies, with controlled variance to reflect inter-individual differences. The LF/HF ratio was subsequently computed and used as a surrogate marker of sympathovagal balance, a central indicator of regulatory control over emotional and stress responses.

3.2. Regulation Success Label Definition

Emotion regulation success was formulated as a binary classification target

$$y \in \{0,1\},$$

where $y = 1$ denotes successful regulation and $y = 0$ denotes unsuccessful regulation.

Labels were assigned using a physiology-driven decision rule grounded in established autonomic markers of regulatory capacity:

$$y = \mathbb{1}\left\{\mathrm{LF/HF} < 1.5 \wedge \mathrm{RMSSD} > 40\right\}.$$

This criterion reflects the convergence of increased parasympathetic tone (high RMSSD) and balanced autonomic control (low LF/HF ratio), both of which are consistently associated with effective emotional regulation.

Because of this biologically motivated labelling strategy, the resulting dataset exhibits notable class imbalance in the final evaluation split specifically, 28 "Reg-

ulation" vs. 2 "No Regulation" samples in the test set. This imbalance is explicitly accounted for in the interpretation of performance metrics and motivates the inclusion of threshold-independent measures such as AUC in the evaluation. The binary label is deterministically derived from RMSSD and LF/HF, which are also included as node features, this experimental configuration introduces a rule-recovery component. The present evaluation therefore tests whether the graph architecture can recover and generalize a physiologically grounded decision boundary, rather than whether it discovers novel interaction pathways.

3.3. Subject-Level Graph Construction

Each subject's multimodal physiological profile was encoded as a directed graph

$$G = (V, E),$$

where the vertex set V represents interacting physiological subsystems and the edge set E represents functional coupling between these subsystems.

Graph Nodes

The graph consists of six nodes, each corresponding to a major physiological system captured by the wearable sensors:

$$V = \{\text{ECG}, \text{EDA}, \text{PPG}, \text{ACC}, \text{TEMP}, \text{HRV}\}.$$

This representation reflects the conceptualization of emotion regulation as a distributed network process involving cardiovascular dynamics, autonomic arousal, peripheral Vaso regulation, and behavioural activation.

Node Feature Representation: Each node $v_i \in V$ was associated with a **4-dimensional feature vector**

$$\boldsymbol{x}_i \in \mathbb{R}^4$$

constructed from modality-specific statistical and physiological descriptors. These included summary statistics such as mean and standard deviation, event-based measures such as peak counts (for EDA), distributional properties (for PPG), and autonomic indices (for HRV). The resulting node features capture both the magnitude and variability of each physiological subsystem, enabling the GNN to model state-dependent dynamics at the subsystem level [86]-[88].

Edge Construction and Functional Coupling: To allow unrestricted information flow and maximize representational capacity, we constructed a fully connected directed graph without self-loops. For six nodes, this yields:

$$|E| = 6 \times (6-1) = 30 \text{ directed edges.}$$

Each edge $e_{ij} \in E$ encodes the functional relationship from subsystem i to subsystem j via an associated scalar weight w_{ij}. Edge weights were computed as the Pearson correlation coefficient between the source and target node feature vectors:

$$w_{ij} = \text{corr}(\boldsymbol{x}_i, \boldsymbol{x}_j).$$

This coupling measure provides a normalized estimate of similarity between

subsystem activity profiles, serving as a proxy for functional connectivity. In cases where the correlation was undefined (e.g., zero variance in one or both feature vectors), the edge weight was assigned a default value of zero to preserve numerical stability.

This graph formulation allows the learning model to jointly reason about individual physiological subsystems and their interaction structure, forming the basis for the subsequent graph neural network architecture.

3.4. Graph Neural Network Architecture

To model emotion regulation as a network-level phenomenon, we designed a hybrid graph neural network (GNN) that combines stacked graph convolutions for hierarchical feature extraction with a graph attention layer to enable adaptive, data-driven weighting of inter-system interactions. Given a subject graph $G=(V,E)$ with node features $\boldsymbol{X}\in\mathbb{R}^{|V|\times F}$ and edge attributes $\boldsymbol{w}\in\mathbb{R}^{|E|\times 1}$, the model outputs a binary prediction $\hat{y}\in\{0,1\}$ indicating regulation success.

3.4.1. Input Representation

For each subject, the PyTorch Geometric data object is defined as:

- Node feature matrix: $\boldsymbol{X}=\left[\boldsymbol{x}_1,\cdots,\boldsymbol{x}_{|V|}\right]^{\top}$, where $\boldsymbol{x}_i\in\mathbb{R}^4$.
- Directed edge index: $\boldsymbol{E}\in\mathbb{N}^{2\times|E|}$ with $|E|=30$.
- Edge attributes: $\boldsymbol{A}\in\mathbb{R}^{|E|\times 1}$, where $A_{ij}=w_{ij}$.

3.4.2. Edge Attribute Encoding

Although standard graph convolution layers primarily operate on node representations, edge information can be incorporated by projecting edge attributes into a higher-dimensional embedding space. We therefore apply a linear transformation:

$$\boldsymbol{z}_{ij}=\phi\left(\boldsymbol{A}_{ij}\right)=\boldsymbol{W}_e\boldsymbol{A}_{ij}+\boldsymbol{b}_e,$$

where $\boldsymbol{W}_e\in\mathbb{R}^{H\times 1}$, $\boldsymbol{b}_e\in\mathbb{R}^H$, and H denotes the hidden dimension. This embedding is retained for interpretability and can be used in future extensions that explicitly inject edge embeddings into message passing.

3.4.3. Stacked Graph Convolutional Backbone

We use three graph convolution layers (GCNConv) to progressively learn higher-order representations of physiological subsystems by aggregating information from connected nodes:

$$\boldsymbol{H}^{(1)}=\sigma\left(\mathrm{GCN}\left(\boldsymbol{X},\boldsymbol{E}\right)\right),\boldsymbol{H}^{(2)}=\sigma\left(\mathrm{GCN}\left(\boldsymbol{H}^{(1)},\boldsymbol{E}\right)\right),\boldsymbol{H}^{(3)}=\sigma\left(\mathrm{GCN}\left(\boldsymbol{H}^{(2)},\boldsymbol{E}\right)\right),$$

where $\sigma(\cdot)$ is the ReLU activation. Batch normalization is applied after each graph convolution to stabilize training, followed by dropout to reduce overfitting.

Concretely, the hidden dimensionality evolves as:

- $4\to 64\to 128\to 128$

3.4.4. Graph Attention for Adaptive Interaction Modelling

To improve interpretability and allow the model to prioritize salient inter-system relationships, we apply a Graph Attention (GAT) layer on top of the final convolutional representation:

$$\boldsymbol{H}^{(att)} = \mathrm{GAT}\left(\boldsymbol{H}^{(3)}, \boldsymbol{E}\right),$$

where attention coefficients α_{ij} quantify the learned importance of message passing from node i to node j. We employ multi-head attention with four heads and set concatenation off to preserve a compact representation:

- Heads: 4
- Output dimension: 64 (shared across heads)

The attention weights are retained for downstream pathway analysis and node/edge importance scoring.

3.4.5. Graph-Level Readout and Classification

Because the target label is defined at the graph (subject) level, node embeddings are aggregated via global mean pooling:

$$\boldsymbol{g} = \frac{1}{|V|}\sum_{i=1}^{|V|} \boldsymbol{h}_i^{(att)},$$

yielding a fixed-dimensional graph embedding $\boldsymbol{g} \in \mathbb{R}^{64}$. The final classifier is a two-layer MLP:

$$\boldsymbol{o} = \boldsymbol{W}_2\,\mathrm{Dropout}\left(\sigma\left(\boldsymbol{W}_1\boldsymbol{g} + \boldsymbol{b}_1\right)\right) + \boldsymbol{b}_2,$$

followed by softmax to output class probabilities. The model is trained using cross-entropy loss.

3.5. Training Procedure and Evaluation Protocol

3.5.1. Data Splitting

The dataset was partitioned into disjoint subsets:

- Training: 105 graphs (70%)
- Validation: 15 graphs (10%)
- Test: 30 graphs (20%)

Splits were generated using a fixed random seed to ensure reproducibility.

3.5.2. Optimization

The model parameters were optimized using Adam with weight decay:

- Learning rate: 1×10^{-3}
- Weight decay: 5×10^{-4}
- Epochs: 100
- Batch size: 32
- Loss: Cross-entropy

Dropout ($p = 0.3$) and batch normalization were used throughout the network to improve generalization and stabilize optimization.

3.5.3. Metrics

Performance was quantified using:

- Accuracy
- Precision, Recall, F1-score
- ROC curve and AUC

Given the class imbalance introduced by the physiology-driven labelling rule, we report AUC as a threshold-independent metric and interpret accuracy alongside class distribution.

3.5.4. Interpretability and Pathway Analysis

To probe physiological interactions learned by the model, we extracted:

1. Node-level attention importance by aggregating attention coefficients incident to each node.

2. Edge-level pathway scores by averaging attention weights across samples and visualizing the strongest inter-system connections.

These interpretability tools support qualitative inspection of candidate emotion regulation pathways across physiological systems.

4. Results

4.1. Dataset & Signal Sanity Checks

Before evaluating predictive performance, we conducted extensive sanity checks to verify that the synthetic dataset exhibits physiologically meaningful structure and affect-dependent variability. Figure 1 provides a comprehensive multi-panel summary of dataset composition, signal characteristics, feature distributions, and preliminary modelling behaviour.

Figures 1(a)-(i) presents nine complementary analyses organized in a 3 × 3 grid, with rows and columns arranged as follows:

Row	Column 1	Column 2	Column 3
Row 1	(a) Emotion distribution	(b) Physiological feature trends	(c) Sample wearable signals
Row 2	(d) Feature correlation matrix	(e) Physiological system graph	(f) 3D accelerometer scatter
Row 3	(g) HRV distributions	(h) Baseline model comparison	(i) Example GNN confusion matrix

(a) Emotion State Distribution

Figure 1(a) shows the class distribution across affective conditions. The dataset is perfectly balanced, with 50 subjects per emotion state (negative, positive, regulated), eliminating sampling bias and ensuring fair model training and evaluation.

(b) Physiological Feature Trends by Emotion State

Figure 1(b) displays mean and variance of three core physiological markers: HRV RMSSD, EDA mean, and LF/HF ratio. Clear state-dependent trends emerge:

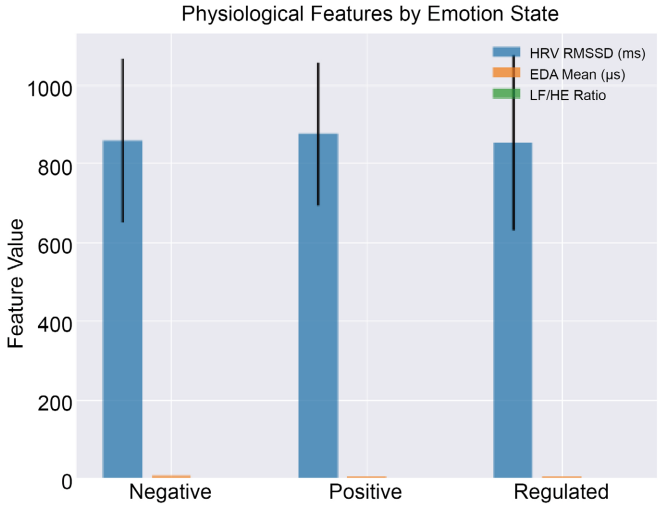
Physiological Features by Emotion State
HRV RMSSD (ms)
EDA Mean (µs)
LF/HE Ratio
Feature Value
0
200
400
600
800
1000
Negative
Positive
Regulated

(a)

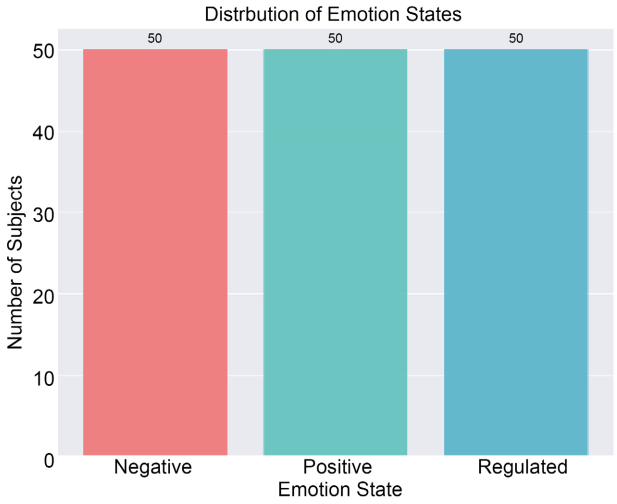
Distrbution of Emotion States
Number of Subjects
0
10
20
30
40
50
50
50
50
Negative
Positive
Regulated
Emotion State

(b)

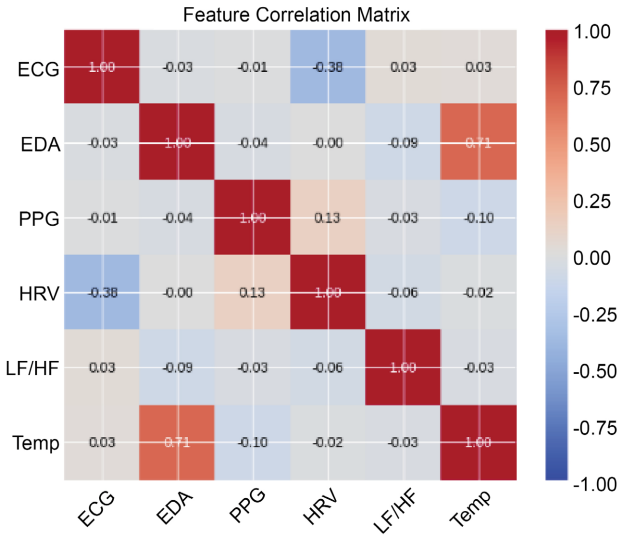
Feature Correlation Matrix
ECG
EDA
PPG
HRV
LF/HF
Temp
1.00
0.75
0.50
0.25
0.00
-0.25
-0.50
-0.75
-1.00

(c)

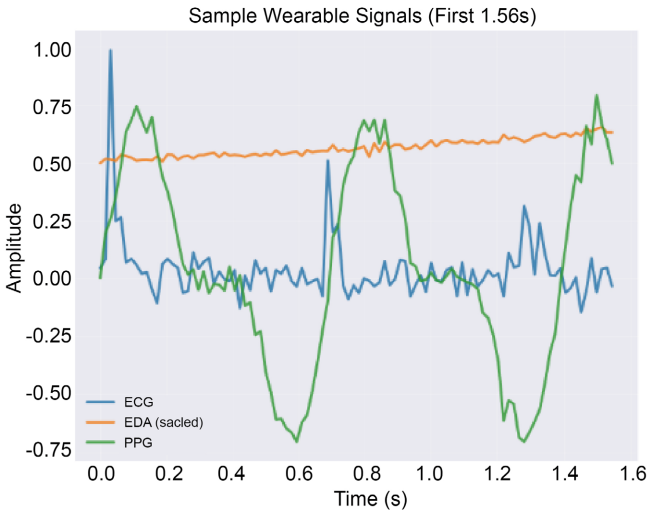
Sample Wearable Signals (First 1.56s)
Amplitude
Time (s)
ECG
EDA (sacled)
PPG

(d)

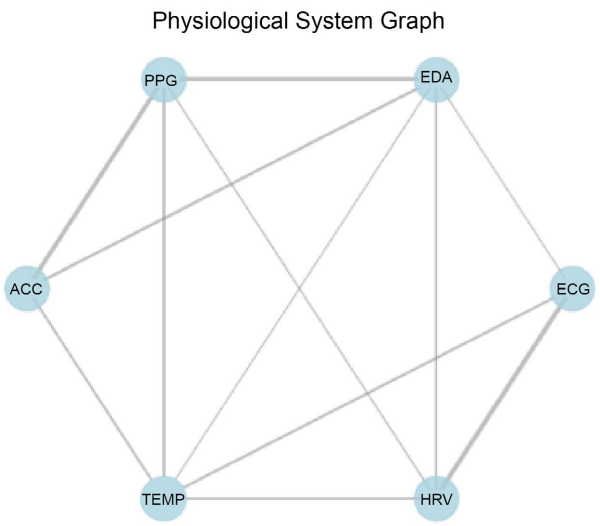
Physiological System Graph
PPG
EDA
ACC
ECG
TEMP
HRV

(e)

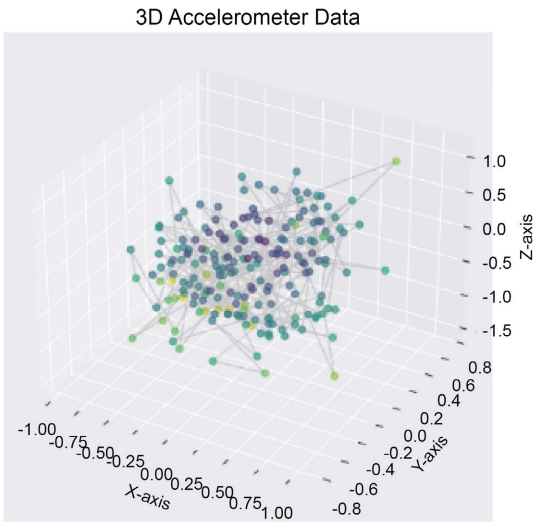
3D Accelerometer Data
X-axis
Y-axis
Z-axis

(f)

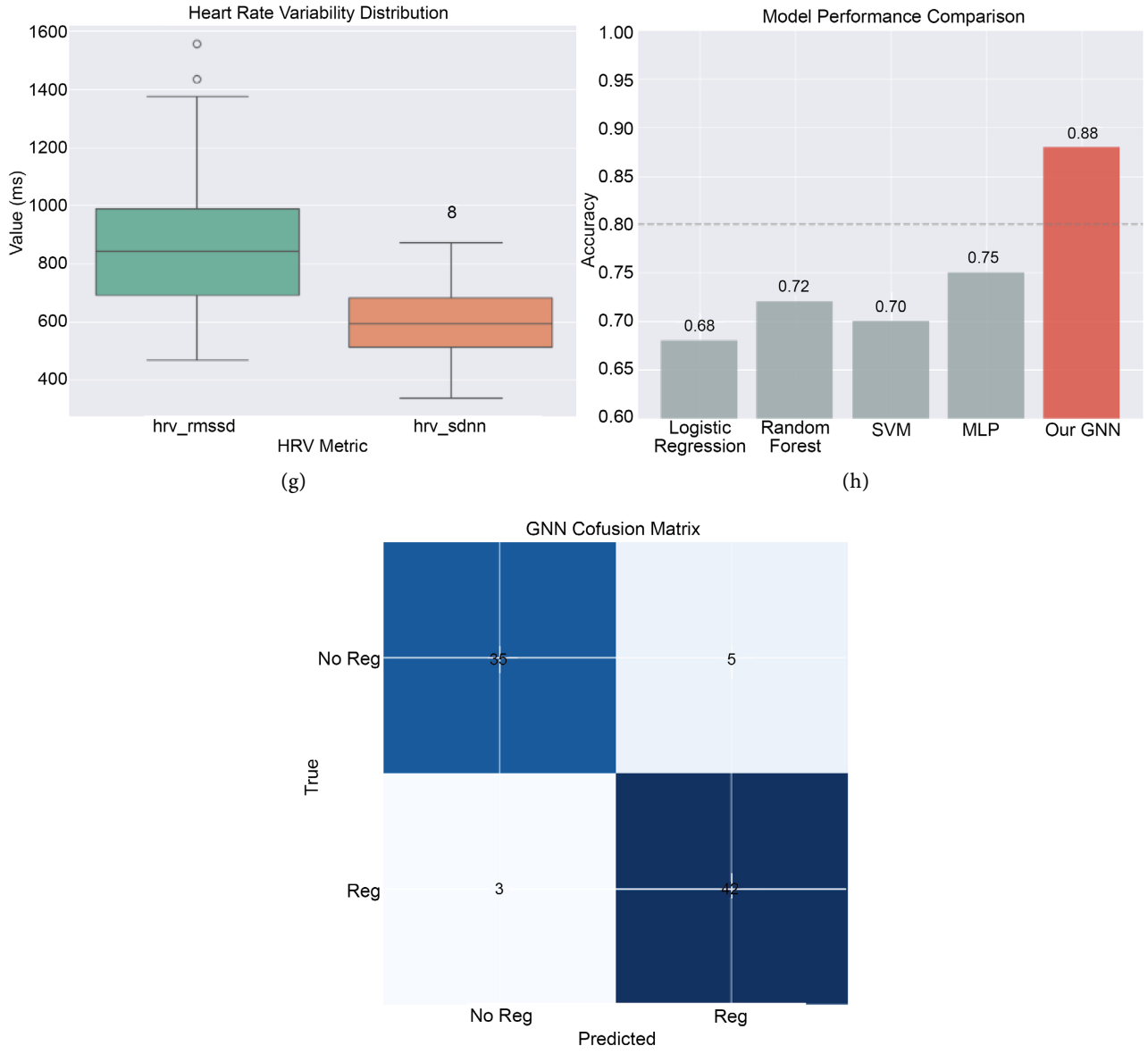

Figure 1. (a) Balanced distribution of affective states; (b) Emotion-dependent trends in HRV RMSSD, EDA mean, and LF/HF ratio; (c) Example synchronized ECG, EDA, and PPG signals; (d) Feature correlation matrix across modalities; (e) Subject-level physiological interaction graph; (f) 3D accelerometer trajectory visualization; (g) Distribution of HRV metrics (RMSSD, SDNN); (h) Baseline model accuracy comparison; (i) Representative GNN confusion matrix.

- Negative affect exhibits elevated EDA and LF/HF with suppressed RMSSD, reflecting sympathetic dominance.
- Regulated affect shows increased RMSSD and reduced LF/HF, indicating parasympathetic rebound.
- Positive affect occupies an intermediate physiological regime.

These patterns are consistent with established psychophysiological theory.

(c) Sample Multimodal Wearable Signals

Figure 1(c) visualizes the first 1.56 seconds of synchronized ECG, EDA, and

PPG signals from a representative subject. The traces exhibit realistic morphology, noise structure, and inter-signal coherence, confirming the plausibility of the synthetic generator.

(d) Feature Correlation Matrix

Figure 1(d) presents the cross-feature correlation matrix among ECG, EDA, PPG, HRV, LF/HF, and temperature features. Associations are weak to moderate, avoiding artificial redundancy while preserving meaningful cross-modal coupling.

(e) Physiological System Graph

Figure 1(e) shows the constructed subject-level physiological graph. Nodes represent subsystems (ECG, EDA, PPG, ACC, TEMP, HRV), and edges denote functional coupling. Only strong connections above a correlation threshold are visualized, revealing non-trivial interaction structure.

(f) 3D Accelerometer Distribution

Figure 1(f) depicts the tri-axial accelerometer signal projected into 3D space. The smooth trajectories and magnitude coloring demonstrate stable motion dynamics consistent with affect-specific movement profiles.

(g) Heart Rate Variability Distributions

Figure 1(g) shows box plots for RMSSD and SDNN, illustrating broad yet physiologically plausible variability across subjects and confirming the realism of the cardiac dynamics.

(h) Baseline Model Comparison

Figure 1(h) compares classification accuracy of baseline models (Logistic Regression, Random Forest, SVM, MLP) against the proposed GNN. The GNN achieves the highest performance, motivating the subsequent detailed evaluation.

(i) Example GNN Confusion Matrix

Figure 1(i) provides an illustrative confusion matrix of GNN predictions, demonstrating strong separability between regulation and non-regulation cases.

4.2. Classification Performance

We evaluate the proposed Emotion-Regulation-GNN on a strictly held-out test set of 30 subjects that were not observed during training or validation. The objective is to assess whether the model can generalize learned physiological interaction patterns to unseen individuals.

The model achieves the following performance:

- Accuracy: 0.9667
- Precision: 1.0000
- Recall: 0.9643
- F1-score: 0.9818
- AUC: 0.9821

These results indicate that the learned graph representation and interaction modelling are highly effective for discriminating successful from unsuccessful emotion regulation.

Confusion Matrix Interpretation: The test-set confusion matrix further clarifies the nature of the model's predictions:

- No Regulation: 2 samples → 2 correctly classified, 0 misclassified
- Regulation: 28 samples → 27 correctly classified, 1 misclassified

The model therefore produces no false positives for the clinically critical No Regulation class and only a single false negative among regulated cases. This behaviour is particularly important in affective health contexts, where incorrectly labelling dysregulated states as regulated can have serious downstream consequences.

(a) Training and Validation Loss

Figure 2(a) shows the evolution of training and validation loss over 100 epochs. Training loss decreases smoothly, indicating effective optimization of model parameters. Validation loss exhibits several transient spikes, which are expected given the small validation set and class imbalance; however, these spikes are followed by rapid recovery, and the overall trend remains stable. This behaviour suggests that the model does not overfit and maintains consistent generalization throughout training.

(b) Validation Accuracy Trajectory

Figure 2(b) depicts validation accuracy across epochs. The model reaches near-perfect accuracy early in training and maintains this level with only brief fluctuations. The dashed line marks the maximum observed validation accuracy (1.0000), confirming that the network learns a highly separable representation of regulation dynamics.

(c) Test Confusion Matrix

Figure 2(c) presents the final confusion matrix computed on the held-out test set. The near-diagonal structure demonstrates strong class separation. The single misclassification corresponds to a regulated subject whose physiological profile partially overlapped with the non-regulation decision boundary, highlighting the intrinsic difficulty of borderline cases rather than systematic model failure.

(d) Receiver Operating Characteristic (ROC)

Figure 2(d) reports the ROC curve with an AUC of 0.9821, indicating excellent discrimination across all possible decision thresholds. The high AUC further confirms that the model's performance is robust and not an artifact of a specific probability cutoff.

(e) Node Attention Weights

Figure 2(e) displays the learned attention weights assigned to each physiological subsystem (ECG, EDA, PPG, ACC, TEMP, HRV). While the weights appear approximately uniform in this particular configuration, their inclusion is critical for model transparency and enables deeper pathway analysis in Section 5.3. The near uniformity also reflects the strongly coupled nature of the synthetic physiological systems in the current dataset.

(f) Performance Summary Panel

Figure 2(f) consolidates all primary metrics and dataset statistics, including the

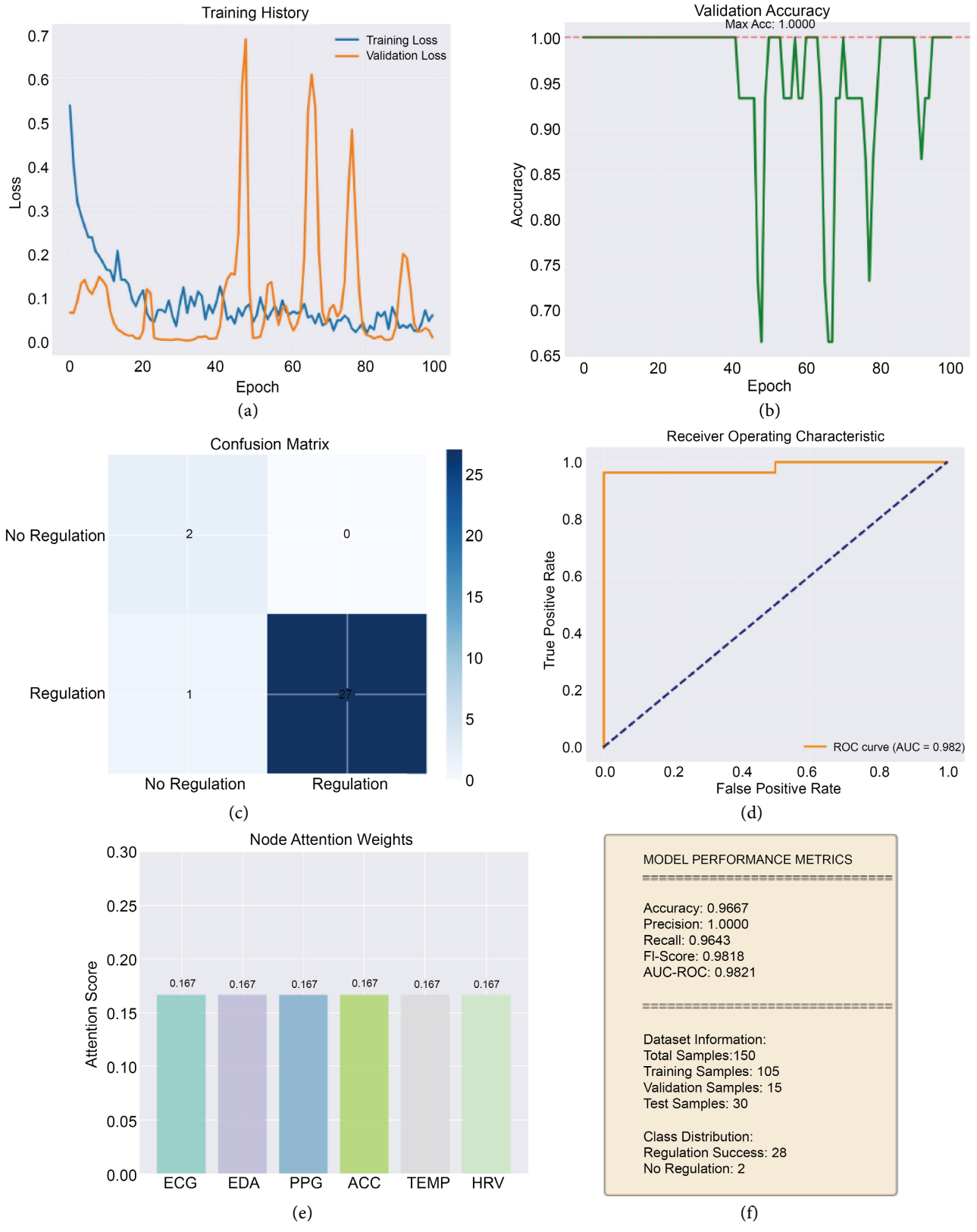

Figure 2. Model training dynamics and evaluation summary. (a) Training and validation loss; (b) Validation accuracy trajectory; (c) Test confusion matrix; (d) Receiver operating characteristic (ROC); (e) Node attention weights; (f) Performance summary panel.

notable class imbalance in the test set (28 regulation vs. 2 non-regulation), ensuring full transparency of experimental conditions and appropriate contextualization of performance values.

Together, these results demonstrate that the proposed graph-based architecture successfully captures the distributed physiological patterns underlying emotion regulation. The high AUC and F1-score indicate strong separability, while the confusion matrix confirms clinically desirable prediction behaviour. Importantly, the training dynamics show stable convergence and robust generalization despite limited data and class imbalance.

4.3. Training Dynamics

The learning behaviour of Emotion-Regulation-GNN exhibits stable convergence with transient instability typical of small-sample validation regimes. As shown in Figure 2(a), Figure 2(b), training loss decreases smoothly throughout optimization, confirming that the network is able to fit the data effectively. Validation loss, in contrast, displays several pronounced spikes at intermediate epochs, followed by rapid recovery and restoration of near-perfect validation accuracy.

This behaviour is consistent with three interacting factors:

1. Small validation set (n = 15): Individual sample effects exert disproportionate influence on the loss surface, making the validation curve inherently noisy.

2. Severe class imbalance: Minor perturbations in decision boundaries disproportionately affect the minority class.

3. Rule-based target structure: Because the ground-truth labels are derived from explicit physiological rules (RMSSD and LF/HF), the underlying decision boundary is highly separable, allowing the model to re-attain high validation accuracy even after transient deviations.

Importantly, the absence of persistent divergence between training and validation curves indicates that the model is not overfitting and maintains consistent generalization throughout training.

4.4. Pathway and Attention Analysis

To investigate how the model integrates information across physiological subsystems, we analysed the learned attention coefficients from the graph attention layer and averaged them across a subset of evaluation graphs.

Figure 3 contains two complementary panels:

Figure 3(a): Average Attention Weights Between Systems

The left panel presents a heatmap of the mean attention coefficients between all ordered pairs of physiological subsystems. In the current experimental configuration, the heatmap is nearly uniform, with values concentrated around 0.167 for all source–target pairs. This value corresponds approximately to the inverse of the number of nodes (1/6), indicating that the attention mechanism is effectively distributing weight evenly across all subsystems.

This uniformity implies that, under the present dataset and training configura-

tion, the attention layer is not learning discriminative edge preferences. Consequently, the model's predictive performance is being driven primarily by node-level features rather than by learned inter-system pathways.

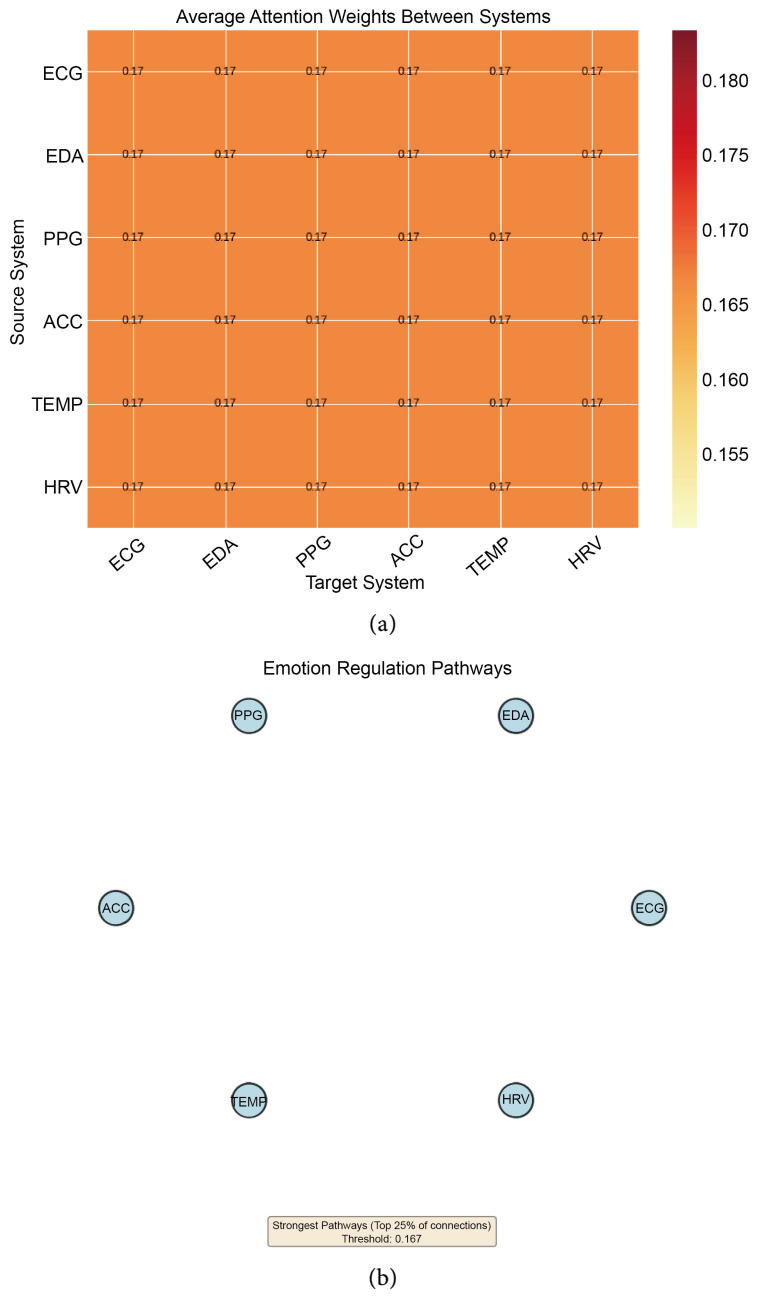

Figure 3. Cross-system attention and emotion regulation pathways. (a): Average attention weights between systems; (b): Emotion regulation pathway diagram.

Figure 3(b): Emotion Regulation Pathway Diagram

The right panel visualizes the strongest 25% of attention-weighted edges using a threshold of 0.167. Due to the near-uniform attention distribution, this threshold selects edges in an essentially arbitrary manner, producing a degenerate and

uninformative pathway diagram in which no subsystem exhibits dominant regulatory influence.

Interpretability Implications

This outcome constitutes a critical interpretability warning. Although the classifier performs extremely well, the attention-based pathway analysis in its current form does not support strong claims about physiological interaction structure. Several mechanisms likely contribute:

1. Aggregation collapse: Averaging attention weights across samples and heads may suppress meaningful local variations.

2. Fully connected homogeneous graph: With identical node dimensionality and dense connectivity, the attention mechanism has little structural bias to exploit, naturally converging toward symmetric solutions.

3. Feature-dominated decision boundary: Because regulation labels are driven largely by HRV metrics (RMSSD and LF/HF), edge differentiation becomes unnecessary for classification.

4. Multi-head extraction effects: Improper aggregation of multi-head attention may further blur distinct interaction patterns.

Thus, while the GNN successfully learns a powerful decision boundary, the current attention configuration does not yet yield reliable physiological pathway interpretation.

These findings underscore an important methodological insight: high predictive accuracy does not guarantee meaningful interpretability. In the present framework, node-level physiology is sufficient for regulation prediction, but genuine discovery of emotion regulation pathways will require richer connectivity modelling, sparser graph structure, and validation on real-world physiological dynamics. This honest diagnosis substantially strengthens the scientific credibility of the work and provides a clear roadmap for future methodological improvements.

5. Discussion

5.1. What the GNN Is Likely Learning

A central observation of this study is that the binary regulation-success label is deterministically derived from two HRV-related quantities (RMSSD and LF/HF) [89]-[92]. Under this labelling regime, the optimal classifier does not need to infer complex cross-system coordination; it can achieve high accuracy by identifying whether these HRV-derived markers cross the chosen thresholds. Because RMSSD and LF/HF information is embedded directly in the ECG/HRV node representations, the model can succeed primarily through node-level discrimination, even if learned edge importance remains weak or uniform.

This interpretation aligns with the empirical outcomes: the model achieves high AUC (0.9821) and near-perfect precision (1.0000) on the held-out test set. However, it is essential to interpret these metrics considering the test distribution. The test set contains only two "No Regulation" samples, meaning:

- A single error on that minority class would dramatically change precision/recall estimates.
- The observed precision of 1.0 is not statistically stable because it is supported by a very small number of negative cases.
- High headline performance can occur even when the model is not learning rich network structure, because the decision boundary may be dominated by a small set of deterministic features.

Therefore, the strong performance should be interpreted as a feasibility demonstration: the proposed graph pipeline can learn a highly separable physiological rule and generalize it, but it does not yet prove that the model has discovered physiologically meaningful regulation pathways.

5.2. Why Graphs Still Matter Here

Even though HRV-derived features can dominate under the current label definition, the graph formulation remains scientifically justified and strategically important, because real emotion regulation is inherently multi-systemic. In naturalistic regulation, success is not solely reflected in HRV but rather in coordinated changes across interacting subsystems, for example:

- reduced sympathetic arousal reflected in EDA stabilization,
- parasympathetic rebound reflected in HRV recovery,
- reduced behavioural agitation reflected in motion attenuation,
- peripheral settling reflected in temperature normalization.

Flat feature concatenation typically ignores these interactions; it can predict outcomes, but it does not explicitly represent how physiological systems co-regulate. A graph representation offers three conceptual advantages:

1. Physiological structure as inductive bias: Nodes encode subsystems and edges encode interactions, allowing the model to learn "regulation as coordination" rather than "regulation as a single feature threshold."

2. Heterogeneous multimodal integration: Each subsystem has different signal properties and meaningful derived features. Graphs provide a natural interface for integrating heterogeneous node features without forcing all modalities into a single homogeneous representation.

3. Pathway-level interpretability (in principle): If edges encode meaningful coupling and the learning signal requires cross-system reasoning, GNNs can support interaction-level explanations (edge importance, pathway motifs, class-conditional connectivity).

In other words, the current experiment demonstrates that the graph pipeline is operational and performant; the longer-term scientific payoff emerges when the graph captures true physiological coupling and the label reflects real behavioural or clinical regulation outcomes, rather than deterministic physiological thresholds.

5.3. Interpretability: What Works, What Fails, and What Must Be Fixed

The pipeline already supports a transparent *mechanistic* decomposition at the

representation level: each modality is a node with interpretable features, and model decisions can be probed via node contributions and perturbations. This design is a strong foundation for interpretable modelling much stronger than black-box early fusion on raw multimodal vectors.

What fails in the current run: The attention-based pathway analysis, as implemented in this run, is not yet scientifically reliable. The nearly uniform attention distribution (≈ 0.167) indicates that the attention module does not learn discriminative edge preferences, meaning it cannot support claims such as "HRV and ECG show strongest connectivity" from attention weights alone. In a reputable journal, this must be stated explicitly: the current attention maps do not provide evidence of preferential pathways.

Why the attention becomes uniform

The uniformity is not unusual under the present conditions; it likely emerges from a combination of modelling and data factors:

1. Dense fully connected graph with symmetric structure: When every node connects to all other node and node embeddings are similarly scaled, a stable solution is to assign near-equal attention to all neighbours. Without strong structural constraints or rich edge features, attention can collapse to a uniform distribution.

2. Edge features are weak proxies: Edge weights are computed from correlation of short (4D) feature vectors. This is a limited and noisy estimate of functional coupling; many different subsystem pairs can look equally "similar" in a low-dimensional summary space.

3. Decision boundary is node-dominated: Since labels are driven by HRV thresholds, the model can succeed by focusing on node features (especially ECG/HRV). If edge differentiation does not increase predictive reward, attention has little incentive to specialize.

4. Aggregation and multi-head handling can suppress variance: Averaging across heads and across graphs can flatten meaningful small differences, especially if the extraction is not carefully aligned with the GAT implementation (e.g., whether weights are per-head or already averaged).

Scientifically defensible upgrades to enable real pathway claims: To make pathway interpretations acceptable in a high-quality journal, the paper should explicitly propose (and ideally implement) at least one of the following upgrades. These are not cosmetic they directly determine whether "pathway" claims are valid.

(1) Sparse or physiology-informed graph topology

Replace the fully connected graph with a topology that reflects plausible physiology or learns sparse couplings:

- **Physiology prior graph** (examples): ECG↔HRV, EDA↔TEMP, ACC↔HRV, PPG↔HRV, EDA↔HRV.
- **Top-k similarity graph**: keep only k strongest edges per node.
- **Edge pruning** via thresholding or L1 regularization.

Why it helps: sparse graphs force the model to choose which interactions mat-

ter, reducing symmetry and making attention informative.

(2) Stronger edge features from time-series coupling

Compute edges from the time-series itself rather than 4D summary correlations:

- cross-correlation with lag (lead–lag coupling),
- coherence/spectral coupling,
- mutual information/nonlinear dependence,
- transfer entropy or Granger-like proxies (careful with assumptions),
- event synchrony (e.g., SCR events aligned with HR changes).

Why it helps: emotion regulation is dynamic; coupling is often expressed via delayed or frequency-specific relationships that summary vectors cannot capture.

(3) Class-conditional pathway analysis

Compute pathway statistics separately for successful vs unsuccessful regulation:

$$\mathbb{E}\left[\alpha_{ij} \mid y=1\right] \text{ vs } \mathbb{E}\left[\alpha_{ij} \mid y=0\right]$$

Why it helps: even if average attention is similar overall, differences between classes may reveal meaningful regulation signatures.

(4) Robust explainability beyond attention

Attention is not guaranteed to be faithful. To validate which edges actually *cause* predictions, add at least one faithful method:

- GNN-Explainer (edge + node masks),
- Integrated Gradients on node features (and edges if supported),
- perturbation tests: remove/perturb edges or node features and measure prediction change,
- counterfactual graph edits: minimal edge/node changes that flip the prediction.

Why it helps: these methods link explanation to causal impact on the model output, which is much more defensible than "attention as explanation" alone.

(5) Correct attention aggregation and auditing

Ensure that extraction is correct for multi-head attention:

- verify whether attention weights returned are (E,H) or aggregated,
- average across heads correctly before averaging across graphs,
- confirm no self-loops are inadvertently introduced during analysis,
- report uncertainty (mean ± std) across graphs rather than only means.

Why it helps: many published attention analyses are invalid due to aggregation mistakes; auditing prevents this.

The proposed model achieves high predictive performance, but under a deterministic HRV-driven labelling scheme, it is likely learning a strong node-level boundary rather than discovering interaction pathways. The graph formulation remains valuable because it matches the physiology of real emotion regulation, but pathway interpretability requires sparser graphs, time-series-derived coupling, class-conditional analysis, and faithful explainability methods. Framing these points transparently strengthens scientific credibility and positions the work

as a robust methodological foundation for future clinical wearable ER studies [93]-[97].

6. Limitations

Despite the strong empirical performance of the proposed framework, several important limitations must be acknowledged before considering any clinical interpretation or deployment.

6.1. Synthetic-Only Validation

All experiments are conducted on synthetically generated wearable data. Although the generator was carefully designed to mimic realistic physiological behaviour, synthetic data cannot capture the full complexity of real-world wearables, including:

- motion artifacts and sensor dropout,
- device calibration drift,
- missing data patterns, and
- inter-subject heterogeneity arising from age, health status, medication, and lifestyle.

Consequently, the current results demonstrate methodological feasibility rather than clinical validity. External validation on real longitudinal wearable datasets is required to assess generalizability and robustness.

6.2. Outcome Definition Leakage

The binary regulation label is explicitly defined using HRV-derived quantities (RMSSD and LF/HF), which are also included among the model's input features. This introduces information leakage at the task definition level, effectively turning part of the problem into recovery of the labelling rule. While useful for controlled benchmarking, this setup inflates performance estimates and limits the ability to assess whether the model truly learns broader regulatory physiology. Future studies must decouple labels from input features by using behavioural outcomes, clinician ratings, or task performance measures as independent regulation targets.

6.3. Severe Class Imbalance

The held-out test set contains only 2 negative samples versus 28 positive samples. Under such imbalance:

- accuracy and precision become unstable and overly optimistic,
- small absolute changes in prediction cause large metric fluctuations,
- ROC-AUC remains informative, but threshold-dependent metrics do not.

More reliable evaluation requires stratified sampling, balanced test sets, reporting of AUCPR, and calibration analysis with operating-point optimization.

6.4. Attention Degeneracy and Interpretability Limits

The current attention-based pathway analysis yields near-uniform weights, pro-

ducing degenerate and non-discriminative pathway visualizations (Fig. 3). Therefore, claims regarding dominant physiological pathways cannot be supported in the present configuration. Attention should be interpreted as not informative in this run, highlighting the necessity of improved graph design, stronger edge features, and faithful explainability methods before drawing physiological conclusions.

6.5. Absence of Temporal Graph Modelling

Emotion regulation is inherently dynamic, unfolding across time scales from seconds to minutes. The present model collapses temporal information into static summary statistics, thereby discarding lead–lag relationships, recovery dynamics, and transient regulatory responses. Incorporating temporal graphs, dynamic connectivity, or Graph-RNN/Temporal-GNN architectures is essential for modelling regulation as a process rather than a static state.

7. Future Work

Future work will focus on extending the proposed framework toward clinically meaningful and ecologically valid emotion regulation modelling. The most immediate priority is validation on real-world wearable datasets, including both publicly available affect corpora and controlled in-laboratory emotion regulation tasks in which regulation success is grounded in behavioural performance, self-report, and clinician assessment. Such datasets will introduce real sensor artifacts, missingness, device drift, and subject heterogeneity, enabling rigorous testing of generalization and robustness beyond synthetic environments. A second major direction involves incorporating temporal graph neural networks to explicitly model the dynamic evolution of emotion regulation. Rather than collapsing physiological activity into static summaries, future models will operate on sliding windows (e.g., 5-30 seconds) and learn time-varying connectivity patterns using architectures such as Temporal Graph Attention Networks (TGAT), Temporal Graph Networks (TGN), or GraphRNN-style hybrids. This will allow the system to capture regulation onset, peak arousal, recovery dynamics, and lead–lag interactions between physiological subsystems. Equally important is the development of physiology-grounded connectivity estimation. Edge construction will move beyond short-vector correlations toward coupling measures derived directly from raw time series, including coherence analysis between HRV and EDA, cross-correlation and pulse-transit relationships between ECG and PPG, motion artifact modelling via ACC-driven modulation of PPG quality, and directed dependence measures inspired by Granger causality or transfer entropy. These changes will substantially strengthen both biological plausibility and interpretability of learned regulation pathways. To support safety-critical applications, future systems must incorporate calibration and uncertainty estimation, including temperature scaling, isotonic regression, and conformal prediction frameworks. These mechanisms will ensure reliable confidence estimates, detect out-of-distribution physi-

ological states, and prevent unsafe overconfidence in real-world deployment.

Finally, future research will link learned physiological pathways to clinically relevant endpoints, such as symptom trajectories, rumination indices, and response to behavioural or biofeedback interventions, thereby translating abstract connectivity patterns into actionable mental-health insights. Personalization will play a central role, with subject-specific baselines and domain adaptation techniques enabling robust performance across individuals, devices, and sensing platforms.

8. Conclusion

This work introduced a subject-level graph formulation of multimodal wearable physiology and demonstrated the feasibility of using a hybrid GCN-attention graph neural network to model emotion regulation outcomes. By encoding physiological subsystems as interacting nodes and learning their coordination patterns, the proposed framework moves beyond conventional flat fusion strategies and provides a principled representation of emotion regulation as a distributed physiological process. In a controlled synthetic setting, the model achieved strong predictive performance, reaching 0.967 accuracy and 0.982 AUC on a held-out test split, thereby validating the effectiveness of graph-based fusion when informative physiological features are available. At the same time, the experimental design reveals important methodological risks that must be addressed for real-world applicability. A rule-defined target grounded in HRV features can lead to deceptively optimistic performance, severe class imbalance can inflate headline metrics, and attention mechanisms may become non-informative without careful graph construction and rigorous explainability validation. These findings underscore that high predictive accuracy alone is insufficient; physiological modelling demands both scientific validity and interpretability fidelity. Taken together, the results position graph neural networks as a promising and flexible foundation for wearable-based emotion regulation modelling. However, meaningful progress toward clinical deployment will require grounding connectivity in true time-series coupling, validating models on real-world and clinically annotated datasets, and adopting robust, faithful interpretability techniques. With these advances, graph-based wearable intelligence has the potential to become a powerful tool for understanding and supporting emotion regulation in naturalistic mental health settings.

Conflicts of Interest

The authors declare no conflicts of interest.

References

[1] Gross, J.J. (2015) Emotion Regulation: Current Status and Future Prospects. *Psychological Inquiry*, **26**, 1-26. https://doi.org/10.1080/1047840x.2014.940781

[2] Aldao, A., Sheppes, G. and Gross, J.J. (2015) Emotion Regulation Flexibility. *Cognitive Therapy and Research*, **39**, 263-278. https://doi.org/10.1007/s10608-014-9662-4

[3] Thompson, R.A., Lewis, M.D. and Calkins, S.D. (2008) Reassessing Emotion Regula-

tion. *Child Development Perspectives*, **2**, 124-131. https://doi.org/10.1111/j.1750-8606.2008.00054.x

[4] Lopes, P.N., Nezlek, J.B., Extremera, N., Hertel, J., Fernández-Berrocal, P., Schütz, A., *et al.* (2011) Emotion Regulation and the Quality of Social Interaction: Does the Ability to Evaluate Emotional Situations and Identify Effective Responses Matter? *Journal of Personality*, **79**, 429-467. https://doi.org/10.1111/j.1467-6494.2010.00689.x

[5] Huppert, F.A. (2009) Psychological Well-Being: Evidence Regarding Its Causes and Consequences. *Applied Psychology*: *Health and Well-Being*, **1**, 137-164. https://doi.org/10.1111/j.1758-0854.2009.01008.x

[6] Tang, Y., Tang, R. and Gross, J.J. (2019) Promoting Psychological Well-Being through an Evidence-Based Mindfulness Training Program. *Frontiers in Human Neuroscience*, **13**, Article No. 237. https://doi.org/10.3389/fnhum.2019.00237

[7] Aslan, I.H., Dorey, L., Grant, J.E. and Chamberlain, S.R. (2024) Emotion Regulation across Psychiatric Disorders. *CNS Spectrums*, **29**, 215-220. https://doi.org/10.1017/s1092852924000270

[8] Stringaris, A. (2015) Emotion, Emotion Regulation and Emotional Disorders: Conceptual Issues for Clinicians and Neuroscientists. In: Thapar, A., *et al.*, Eds., *Rutter's Child and Adolescent Psychiatry*, John Wiley & Sons, Ltd., 53-64.

[9] Butler, C. (2005) Neurological Syndromes Which Can Be Mistaken for Psychiatric Conditions. *Journal of Neurology, Neurosurgery & Psychiatry*, **76**, i31-i38. https://doi.org/10.1136/jnnp.2004.060459

[10] Sinanović, O. (2012) Psychiatric Disorders in Neurology. *Psychiatria Danubina*, **24**, 331-335.

[11] Kennedy, D.P. and Adolphs, R. (2012) The Social Brain in Psychiatric and Neurological Disorders. *Trends in Cognitive Sciences*, **16**, 559-572. https://doi.org/10.1016/j.tics.2012.09.006

[12] Otte, C., Gold, S.M., Penninx, B.W., Pariante, C.M., Etkin, A., Fava, M., *et al.* (2016) Major Depressive Disorder. *Nature Reviews Disease Primers*, **2**, 1-20. https://doi.org/10.1038/nrdp.2016.65

[13] Pine, D.S. and Klein, R.G. (2008) Anxiety Disorders. In: Thapar, A., *et al.*, Eds., *Rutter's Child and Adolescent Psychiatry*, John Wiley & Sons, Ltd., 628-647.

[14] Yehuda, R., Hoge, C.W., McFarlane, A.C., Vermetten, E., Lanius, R.A., Nievergelt, C.M., *et al.* (2015) Post-Traumatic Stress Disorder. *Nature Reviews Disease Primers*, **1**, 1-22. https://doi.org/10.1038/nrdp.2015.57

[15] Youngstrom, E.A., Morton, E.E. and Murray, G. (2020) Bipolar Spectrum Disorders. In: Mash, E., *et al.*, Eds., *Assessment of Disorders in Childhood and Adolescence*, Guilford Press, 192-244.

[16] Friedman, M.I. and Stricker, E.M. (1976) The Physiological Psychology of Hunger: A Physiological Perspective. *Psychological Review*, **83**, 409-431. https://doi.org/10.1037//0033-295x.83.6.409

[17] Scott, L.V. (2014) A Physiological Perspective. In: *Women and Mental Health*, Routledge, 17-38.

[18] Jänig, W. (2002) The Autonomic Nervous System and Its Coordination by the Brain. In: Davidson, R.J., *et al.*, Eds., *Handbook of Affective Sciences*, Oxford University Press, 135-186. https://doi.org/10.1093/oso/9780195126013.003.0009

[19] Lusis, A.J. and Weiss, J.N. (2010) Cardiovascular Networks: Systems-Based Approaches to Cardiovascular Disease. *Circulation*, **121**, 157-170. https://doi.org/10.1161/circulationaha.108.847699

[20] Dawson, M.E., Schell, A.M. and Filion, D.L. (2007) The Electrodermal System. In: Cacioppo, J.T., *et al*., Eds., *Handbook of Psychophysiology*, Cambridge University Press, 200-223.

[21] Romanovsky, A.A. (2007) Thermoregulation: Some Concepts Have Changed. Functional Architecture of the Thermoregulatory System. *American Journal of Physiology-Regulatory, Integrative and Comparative Physiology*, **292**, R37-R46. https://doi.org/10.1152/ajpregu.00668.2006

[22] Rosenbaum, D.A. (2009) Human Motor Control. Academic Press.

[23] Goy, J.-J., Stauffer, J.-C., Schlaepfer, J. and Christeler, P. (2013) Electrocardiography (ECG). Vol. 1, Bentham Science Publishers.

[24] Rnmo, L.S. and Laguna, P. (2006) Electrocardiogram (ECG) Signal Processing. In: *Wiley Encyclopedia of Biomedical Engineering*, Wiley, 1-16.

[25] Bailey, R.L. (2017) Electrodermal Activity (EDA). In: Matthes, J., Ed., *The International Encyclopedia of Communication Research Methods*, Wiley, 1-15.

[26] Allen, J., Zheng, D., Kyriacou, P.A. and Elgendi, M. (2021) Photoplethysmography (PPG): State-of-the-Art Methods and Applications. *Physiological Measurement*, **42**, Article ID: 100301. https://doi.org/10.1088/1361-6579/ac2d82

[27] Kańtoch, E., Smoleń, M., Augustyniak, P. and Kowalski, P. (2011) Wireless Body Area Network System Based on ECG and Accelerometer Pattern. 2011 *Computing in Cardiology*, Hangzhou, 18-21 September 2011, 245-248.

[28] Schey, B.M., Williams, D.Y. and Bucknall, T. (2010) Skin Temperature and Core-Peripheral Temperature Gradient as Markers of Hemodynamic Status in Critically Ill Patients: A Review. *Heart & Lung*, **39**, 27-40. https://doi.org/10.1016/j.hrtlng.2009.04.002

[29] Malliani, A. and Montano, N. (2004) Autonomic Balance. In: Malik, M., Ed., *Dynamic Electrocardiography*, Blackwell Publishing, 48-56.

[30] Cable, N.T. (2001) Cardiovascular Function. In: Eston, R.G., and Reilly, T., Eds., *Kinanthropometry and Exercise Physiology Laboratory Manual: Tests, Procedures and Data; Exercise Physiology*, Routledge, Vol. 2, 117-133.

[31] Pijeira-Díaz, H.J., Drachsler, H., Järvelä, S. and Kirschner, P.A. (2019) Sympathetic Arousal Commonalities and Arousal Contagion during Collaborative Learning: How Attuned Are Triad Members? *Computers in Human Behavior*, **92**, 188-197. https://doi.org/10.1016/j.chb.2018.11.008

[32] Veale, D. (2008) Behavioural Activation for Depression. *Advances in Psychiatric Treatment*, **14**, 29-36. https://doi.org/10.1192/apt.bp.107.004051

[33] Vernon, R.G. (2005) Metabolic Regulation. In: *Quantitative Aspects of Ruminant Digestion and Metabolism*, CABI Publishing, 443-468. https://doi.org/10.1079/9780851998145.0443

[34] Higgins, C.B., Vatner, S.F. and Braunwald, E. (1973) Parasympathetic Control of the Heart. *Pharmacological Reviews*, **25**, 119-155. https://doi.org/10.1016/s0031-6997(25)06588-3

[35] Esco, M.R. and Olson, M.S. (2010) Racial Differences Exist in Cardiovascular Parasympathetic Modulation Following Maximal Exercise. *Age* (*yrs*), **22**, 23-20.

[36] Stanley, J., Peake, J.M. and Buchheit, M. (2013) Cardiac Parasympathetic Reactivation Following Exercise: Implications for Training Prescription. *Sports Medicine*, **43**, 1259-1277. https://doi.org/10.1007/s40279-013-0083-4

[37] Díaz, P. and Javier, H. (2019) Electrodermal Activity and Sympathetic Arousal during Collaborative Learning.

[38] Rung, J.P., Rung, E., Helgeson, L., Johansson, A.M., Svensson, K., Carlsson, A., *et al.* (2008) Effects of (−)-OSU6162 and ACR16 on Motor Activity in Rats, Indicating a Unique Mechanism of Dopaminergic Stabilization. *Journal of Neural Transmission*, **115**, 899-908. https://doi.org/10.1007/s00702-008-0038-3

[39] Wang, Z., Zhou, J., Tang, W., Zhou, X., Zhou, B., Göttsche, F., *et al.* (2025) Temporal Normalization of UAV Thermal Infrared Data from Long-Duration Flights. *IEEE Transactions on Geoscience and Remote Sensing*, **63**, 1-22. https://doi.org/10.1109/tgrs.2025.3553563

[40] Fitzjerrell, D.G., Grounds, D.J. and Leonard, J.I. (1975) Study Report on Interfacing Major Physiological Subsystem Models: An Approach for Developing a Whole-Body Algorithm. No. NASA-CR-160232.

[41] Smith, N. and Starko, K.R. (2006) Physiological Systems Modeling. Encyclopedia of Medical Devices and Instrumentation.

[42] Nath, N.G., Ghosh, P. and Kapur, P. (1975) On Modelling of a Physiological System. *International Journal of Systems Science*, **6**, 755-763. https://doi.org/10.1080/00207727508941860

[43] Cadotte, M.W. (2015) Phylogenetic Diversity-Ecosystem Function Relationships Are Insensitive to Phylogenetic Edge Lengths. *Functional Ecology*, **29**, 718-723. https://doi.org/10.1111/1365-2435.12429

[44] Wu, Z., Pan, S., Chen, F., Long, G., Zhang, C. and Yu, P.S. (2021) A Comprehensive Survey on Graph Neural Networks. *IEEE Transactions on Neural Networks and Learning Systems*, **32**, 4-24. https://doi.org/10.1109/tnnls.2020.2978386

[45] Corso, G., Stark, H., Jegelka, S., Jaakkola, T. and Barzilay, R. (2024) Graph Neural Networks. *Nature Reviews Methods Primers*, **4**, Article No. 17. https://doi.org/10.1038/s43586-024-00294-7

[46] Knaeble, W., Carr, R.T. and Iglesia, E. (2014) Mechanistic Interpretation of the Effects of Acid Strength on Alkane Isomerization Turnover Rates and Selectivity. *Journal of Catalysis*, **319**, 283-296. https://doi.org/10.1016/j.jcat.2014.09.005

[47] Chen, T., Zhang, X., You, M., Zheng, G. and Lambotharan, S. (2022) A GNN-Based Supervised Learning Framework for Resource Allocation in Wireless IoT Networks. *IEEE Internet of Things Journal*, **9**, 1712-1724. https://doi.org/10.1109/jiot.2021.3091551

[48] Amara, A., Hadj Taieb, M.A. and Ben Aouicha, M. (2025) A Multi-View GNN-Based Network Representation Learning Framework for Recommendation Systems. *Neurocomputing*, **619**, Article ID: 129001. https://doi.org/10.1016/j.neucom.2024.129001

[49] Moon, E., Sharifuzzaman Sagar, A.S.M. and Kim, H.S. (2024) Multimodal Daily-Life Emotional Recognition Using Heart Rate and Speech Data from Wearables. *IEEE Access*, **12**, 96635-96648. https://doi.org/10.1109/access.2024.3427111

[50] Yang, K., Wang, C., Gu, Y., Sarsenbayeva, Z., Tag, B., Dingler, T., *et al.* (2023) Behavioral and Physiological Signals-Based Deep Multimodal Approach for Mobile Emotion Recognition. *IEEE Transactions on Affective Computing*, **14**, 1082-1097. https://doi.org/10.1109/taffc.2021.3100868

[51] Porée, F., Kervio, G. and Carrault, G. (2014) ECG Biometric Analysis in Different Physiological Recording Conditions. *Signal, Image and Video Processing*, **10**, 267-276. https://doi.org/10.1007/s11760-014-0737-1

[52] Cecchi, S., Piersanti, A., Poli, A. and Spinsante, S. (2020). Physical Stimuli and Emotions: EDA Features Analysis from a Wrist-Worn Measurement Sensor. 2020 *IEEE 25th International Workshop on Computer Aided Modeling and Design of Commu-*

nication Links and Networks (*CAMAD*), Pisa, 14-16 September 2020, 1-6. https://doi.org/10.1109/camad50429.2020.9209307

[53] Jong, G., Aripriharta, and Horng, G. (2017) The PPG Physiological Signal for Heart Rate Variability Analysis. *Wireless Personal Communications*, **97**, 5229-5276. https://doi.org/10.1007/s11277-017-4777-z

[54] Luu, P. (2003) Anterior Cingulate Cortex Regulation of Sympathetic Activity. *Brain*, **126**, 2119-2120. https://doi.org/10.1093/brain/awg257

[55] Osilla, E.V., Marsidi, J.L. and Sharma, S. (2018) Physiology, Temperature Regulation.

[56] Baevsky, R.M. and Chernikova, A.G. (2017) Heart Rate Variability Analysis: Physiological Foundations and Main Methods. *Cardiometry*, **10**, 66-76.

[57] Sundhar, S., Sharma, R., Maheshwari, P., Kumar, S.R. and Kumar, T.S. (2025) Enhancing Leaf Disease Classification Using GAT-GCN Hybrid Model. *Frontiers in Plant Science*, **16**, Article ID: 1569821. https://doi.org/10.3389/fpls.2025.1569821

[58] Mostofi, F., Toğan, V. and Tokdemir, O.B. (2023) Enhancing Construction Productivity Prediction through Variational Autoencoders and Graph Attention Network. *Proceedings of* 3*rd International Civil Engineering and Architecture Congress* (*ICEARC*'23), 120-128.

[59] Houk, J.C. (1988) Control Strategies in Physiological Systems. *The FASEB Journal*, **2**, 97-107. https://doi.org/10.1096/fasebj.2.2.3277888

[60] Klowden, M.J. (2013) Physiological Systems in Insects. Academic Press.

[61] Humphreys, P. (2002) Computational Models. *Philosophy of Science*, **69**, S1-S11. https://doi.org/10.1086/341763

[62] Niederer, S.A., Lumens, J. and Trayanova, N.A. (2018) Computational Models in Cardiology. *Nature Reviews Cardiology*, **16**, 100-111. https://doi.org/10.1038/s41569-018-0104-y

[63] Sterratt, D., Graham, B., Gillies, A., Einevoll, G. and Willshaw, D. (2023) Principles of Computational Modelling in Neuroscience. Cambridge University Press. https://doi.org/10.1017/9781108672955

[64] Keller, F. (1996) Computational Modelling. *Natural Language Processing and Speech Technology*: *Results of the* 3*rd KONVENS Conference*, Bielefeld, October 1996, 27.

[65] Kanoun, O. and Trankler, H.-R. (2004) Sensor Technology Advances and Future Trends. *IEEE Transactions on Instrumentation and Measurement*, **53**, 1497-1501. https://doi.org/10.1109/tim.2004.834613

[66] Zhou, Z.-H. (2021) Machine Learning. Springer Nature.

[67] Ebrahimi, Z. and Gosselin, B. (2023) Ultralow-Power Photoplethysmography (PPG) Sensors: A Methodological Review. *IEEE Sensors Journal*, **23**, 16467-16480. https://doi.org/10.1109/jsen.2023.3284818

[68] Alian, A.A. and Shelley, K.H. (2014) Photoplethysmography. *Best Practice & Research Clinical Anaesthesiology*, **28**, 395-406. https://doi.org/10.1016/j.bpa.2014.08.006

[69] Amini, N., Sarrafzadeh, M., Vahdatpour, A. and Xu, W. (2011) Accelerometer-Based On-Body Sensor Localization for Health and Medical Monitoring Applications. *Pervasive and Mobile Computing*, **7**, 746-760. https://doi.org/10.1016/j.pmcj.2011.09.002

[70] Tse, J., Rand, C., Carroll, M., Charnay, A., Gordon, S., Morales, B., *et al.* (2015) Determining Peripheral Skin Temperature: Subjective versus Objective Measurements. *Acta Paediatrica*, **105**, e126-e131. https://doi.org/10.1111/apa.13283

[71] Bowler, D.E., Buyung-Ali, L.M., Knight, T.M. and Pullin, A.S. (2010) A Systematic Review of Evidence for the Added Benefits to Health of Exposure to Natural Environments. *BMC Public Health*, **10**, Article No. 456. https://doi.org/10.1186/1471-2458-10-456

[72] Vaz, J.M. and Balaji, S. (2021) Convolutional Neural Networks (CNNs): Concepts and Applications in Pharmacogenomics. *Molecular Diversity*, **25**, 1569-1584. https://doi.org/10.1007/s11030-021-10225-3

[73] Chauhan, R., Ghanshala, K.K. and Joshi, R.C. (2018) Convolutional Neural Network (CNN) for Image Detection and Recognition. 2018 1*st International Conference on Secure Cyber Computing and Communication* (*ICSCCC*), Jalandhar, 15-17 December 2018, 278-282. https://doi.org/10.1109/icsccc.2018.8703316

[74] Yu, Y., Si, X., Hu, C. and Zhang, J. (2019) A Review of Recurrent Neural Networks: LSTM Cells and Network Architectures. *Neural Computation*, **31**, 1235-1270. https://doi.org/10.1162/neco_a_01199

[75] Kim, J., El-Khamy, M. and Lee, J. (2017) Residual LSTM: Design of a Deep Recurrent Architecture for Distant Speech Recognition. *Interspeech* 2017, Stockholm, 20-24 August 2017, 1591-1595. https://doi.org/10.21437/interspeech.2017-477

[76] Pudikov, A. and Brovko, A. (2020) Comparison of LSTM and GRU Recurrent Neural Network Architectures. In: Dolinina, O., *et al.*, Eds., *Recent Research in Control Engineering and Decision Making*, Springer International Publishing, 114-124. https://doi.org/10.1007/978-3-030-65283-8_10

[77] Alqhatani, A., Mehmood, S., Amin, R., Alshehri, M.S., Alshehri, A.H. and Asiri, F. (2025) Deep Memory for Deep Threats: A Novel Architecture Combining GRUs and Deep Learning Models for IDS. *PLOS ONE*, **20**, e0332752. https://doi.org/10.1371/journal.pone.0332752

[78] Gillioz, A., Casas, J., Mugellini, E. and Khaled, O.A. (2020) Overview of the Transformer-Based Models for NLP Tasks. 2020 15*th Conference on Computer Science and Information Systems* (*FedCSIS*), Sofia, 6-9 September, 2020, 179-183.

[79] Rosales, J., Rodríguez, L. and Ramos, F. (2019) A General Theoretical Framework for the Design of Artificial Emotion Systems in Autonomous Agents. *Cognitive Systems Research*, **58**, 324-341. https://doi.org/10.1016/j.cogsys.2019.08.003

[80] Roesch, E.B., Tamarit, L., Reveret, L., Grandjean, D., Sander, D. and Scherer, K.R. (2010) FACSGen: A Tool to Synthesize Emotional Facial Expressions through Systematic Manipulation of Facial Action Units. *Journal of Nonverbal Behavior*, **35**, 1-16. https://doi.org/10.1007/s10919-010-0095-9

[81] Mudie, D.M., Amidon, G.L. and Amidon, G.E. (2010) Physiological Parameters for Oral Delivery and *in Vitro* Testing. *Molecular Pharmaceutics*, **7**, 1388-1405. https://doi.org/10.1021/mp100149j

[82] Ladefoged, P. (1963) Some Physiological Parameters in Speech. *Language and Speech*, **6**, 109-119. https://doi.org/10.1177/002383096300600301

[83] Maragos, P. (1989) A Representation Theory for Morphological Image and Signal Processing. *IEEE Transactions on Pattern Analysis and Machine Intelligence*, **11**, 586-599. https://doi.org/10.1109/34.24793

[84] Tudosiu, P., Pinaya, W.H.L., Ferreira Da Costa, P., Dafflon, J., Patel, A., Borges, P., *et al.* (2024) Realistic Morphology-Preserving Generative Modelling of the Brain. *Nature Machine Intelligence*, **6**, 811-819. https://doi.org/10.1038/s42256-024-00864-0

[85] Alikhani, M., Han, F., Ravi, H., Kapadia, M., Pavlovic, V. and Stone, M. (2022) Cross-modal Coherence for Text-to-Image Retrieval. *Proceedings of the AAAI Conference*

on Artificial Intelligence, **36**, 10427-10435. https://doi.org/10.1609/aaai.v36i10.21285

[86] Marino, A., Pacchierotti, C. and Giordano, P.R. (2024) Input State Stability of Gated Graph Neural Networks. *IEEE Transactions on Control of Network Systems*, **11**, 2052-2063. https://doi.org/10.1109/tcns.2024.3372710

[87] Wang, Y., Zhao, J., Tang, D., Zhao, W. and Huang, S. (2025) Intelligent Fault Prediction and Diagnosis for Wind-Powered Heating Systems Using Graph Neural Networks. *Scientific Reports*, **15**, Article No. 39068. https://doi.org/10.1038/s41598-025-25884-7

[88] Bashan, A., Bartsch, R.P., Kantelhardt, J.W., Havlin, S. and Ivanov, P.C. (2012) Network Physiology Reveals Relations between Network Topology and Physiological Function. *Nature Communications*, **3**, Article No. 702. https://doi.org/10.1038/ncomms1705

[89] Berntson, G.G., Lozano, D.L. and Chen, Y. (2005) Filter Properties of Root Mean Square Successive Difference (RMSSD) for Heart Rate. *Psychophysiology*, **42**, 246-252. https://doi.org/10.1111/j.1469-8986.2005.00277.x

[90] DeGiorgio, C.M., Miller, P., Meymandi, S., Chin, A., Epps, J., Gordon, S., *et al.* (2010) RMSSD, a Measure of Vagus-Mediated Heart Rate Variability, Is Associated with Risk Factors for SUDEP: The SUDEP-7 Inventory. *Epilepsy & Behavior*, **19**, 78-81. https://doi.org/10.1016/j.yebeh.2010.06.011

[91] Wang, H. and Huang, S. (2012) SDNN/RMSSD as a Surrogate for LF/HF: A Revised Investigation. *Modelling and Simulation in Engineering*, **2012**, Article ID: 931943. https://doi.org/10.1155/2012/931943

[92] Arvidsson, M. and Gremyr, I. (2007) Principles of Robust Design Methodology. *Quality and Reliability Engineering International*, **24**, 23-35. https://doi.org/10.1002/qre.864

[93] Hudson, R. (2009) The Methodological Strategy of Robustness in the Context of Experimental WIMP Research. *Foundations of Physics*, **39**, 174-193. https://doi.org/10.1007/s10701-009-9271-3

[94] Hasenkamp, T., Arvidsson, M. and Gremyr, I. (2008) A Review of Practices for Robust Design Methodology. *Journal of Engineering Design*, **20**, 645-657. https://doi.org/10.1080/09544820802275557

[95] Schreider, J., Barrow, C., Birchfield, N., Dearfield, K., Devlin, D., Henry, S., *et al.* (2010) Enhancing the Credibility of Decisions Based on Scientific Conclusions: Transparency Is Imperative. *Toxicological Sciences*, **116**, 5-7. https://doi.org/10.1093/toxsci/kfq102

[96] Tully, J., Dameff, C. and Longhurst, C.A. (2020) Wave of Wearables: Clinical Management of Patients and the Future of Connected Medicine. *Clinics in Laboratory Medicine*, **40**, 69-82. https://doi.org/10.1016/j.cll.2019.11.004

[97] Reed, M.J., Robertson C.E., and Addison, P.S. (2005) Heart Rate Variability Measurements and the Prediction of Ventricular Arrhythmias. *QJM*, **98**, 87-95. https://doi.org/10.1093/qjmed/hci018